On the intermetallic constituents in the sodium-induced edge cracking of hot-rolled AA5182 aluminum alloys

Mohammadreza Mofarrehi, Mousa Javidani, X.-Grant Chen *

Department of Applied Science, University of Quebec at Chicoutimi, Saguenay, QC, G7H 2B1 Canada

* Corresponding author: X.-Grant Chen (xgrant_chen@uqac.ca)

Abstract

The productivity and recovery of hot-rolled Al-Mg-Mn sheets often suffer from sodium-induced edge cracking. In this study, AA5182 ingots with different levels of Na were prepared by direct-chill (DC) casting, and were then subsequently subjected to homogenization and hot-rolling processes. The edge crack occurrence during hot rolling in the pass #11 (84% reduction) and pass #18 (96% reduction) was investigated, with special attention paid to the impact of intermetallic constituents in the ingot subsurface region, where all edge cracks were initiated. Correlations between the susceptibility to edge cracking, enriched intermetallic constituents in the inverse segregation zone, Mg_2Si cavitation, meniscus bands, and Na contamination were observed. The results revealed that Fe-rich intermetallic particles were not involved in crack formation, while Mg_2Si particles had a strong tendency to debond from the Al matrix and form cavities at the edges of the rolled strip. The higher the Na content, the more severe the Mg_2Si cavitation, and consequently, the higher the susceptibility to edge cracking. Numerous debonded Mg_2Si particles contaminated with Na in the subsurface region provided favorable conditions for crack initiation and propagation. The role of the meniscus bands on the large and profound edge cracks was also elaborated.

Keywords: AA5182 aluminum alloys; Edge cracking; Hot rolling; Na contamination; Mg_2Si cavitation

1. Introduction

Owing to their high strength-to-weight ratio, excellent corrosion resistance, good formability and weldability, Al-Mg sheets are increasingly used to manufacture lightweight parts of the car body and chassis in the automotive industry [1-3]. However, the productivity, recovery, and quality of Al-Mg sheet products often suffer from edge cracking during hot rolling [4–6]. In commercial Al-Mg alloys, Na is a common undesirable impurity; even a trace amount of Na can jeopardize productivity by contributing to severe edge cracking. However, the presence of Na in the order of ppm is inevitable in the casting process. Commercial Al-Mg sheet products are usually fabricated through DC casting, homogenization, hot rolling, and cold rolling. Since all edge cracks

initiate at the surface of DC-cast ingots, the microstructural aspects in the subsurface region of DC ingots and their relationship with the impact of Na are of great technical interest.

In DC-cast ingot products, an enriched layer composed of a large amount of solutes and intermetallic constituents is formed in the subsurface region by inverse segregation [7,8]. Through the inverse segregation and volume contraction, the solute-rich liquid moves in the opposite direction of the solidification front by penetrating into the network of solidifying dendrites in the mushy zone [8]. Owing to the fluctuation of the melt pressure, the movement of the liquid level, and the surface tension of the liquid, meniscus bands also form on the ingot surface at regular intervals, through which the inverse segregation is further extended toward the bulk [9,10]. Prior to hot rolling, the ingot is homogenized, and the surface zone is scalped off from the rolling faces of the ingot. However, the homogenization process cannot completely remove the effect of inverse segregation and the meniscus bands, as some intermetallics are insoluble or only partially soluble. Furthermore, in industrial practices, the short sides of Al DC-cast ingots are usually not scalped prior to rolling. Consequently, the enriched layer of intermetallics in the subsurface region could potentially be favorable sites for edge cracking.

The detrimental influence of Na on the embrittlement and edge cracking of Al-Mg alloys has been long recognized and investigated. Ransley and Talbot [11] first investigated the embrittlement of Al–Mg–Si alloys and reported that hot ductility was strongly impaired at high Na levels. Several researchers reported that the high-temperature embrittlement of Al-Mg alloys was caused by the segregation of trace Na to grain boundaries; hence, grain boundary weakening was considered as the root cause of edge cracks [12–16]. Horikawa et al. [16] examined the effect of Na on high-temperature embrittlement by measuring the reduction of area during tensile testing of Al–5Mg alloys containing different levels of Na, in the range of 0.01-2 ppm. Trace Na was detected by glow discharge mass spectrometry and was assumed to segregate to the grain boundaries in the form of free Na atoms. However, Lynch [17] believed that the hypothesis of grain boundary segregation was doubtful and suggested that the high-temperature embrittlement might be due to the formation of low melting point Na-rich phases or particles after comparison with other Al alloys. Simensen and Sodervall [18] investigated the trace elements in Al-4.8Mg-0.3Mn DC-cast ingots and found that the impurities (e.g., Na, Ca, etc.) were segregated and enriched in the cast surface layer of DC ingots, forming a number of Na particles on the surfaces of intermetallic particles. Through a thermodynamic simulation, Zhang et al. [19] reported that Na in Al-Mg system could form a so-called liquid-2 phase at fairly low-Na concentrations, which had a very low melting point. During hot rolling, it transformed into a liquid and caused low ductility at the grain boundaries or at other phase boundaries. It was concluded that the higher the Na content in the alloy, the greater the volume of this liquid phase, and consequently the higher the embrittlement. Hosokawa et al. [20] studied the development of cavitation on the periphery of Mg_2Si particles during large-scale tensile deformation in an Al-4.5Mg alloy, and found that the volume fraction of Mg_2Si cavities significantly increased with increasing strain, and that Mg_2Si particles were not beneficial for hot workability by promoting cavitation at high temperatures.

Despite numerous investigations, the mechanisms of Na on embrittlement and edge cracking in Al–Mg alloys have not been fully understood. In the present work, great efforts have been made to characterize the microstructure in the subsurface region of DC-cast ingots, where the enriched intermetallic constituents were segregated and induced crack initiation. Furthermore, the interaction of the intermetallics with Na, as well as the combined effect of microconstituents and hot-rolling process on edge cracking susceptibility, were studied.

2. Experimental procedure

AA5182 alloys with two different levels of Na were prepared by DC casting for pilot-scale casting and hot rolling trials; one alloy had an Na content of less than 0.5 ppm, and the other consisted of more than 1 ppm Na. The former is denoted hereafter as LS (which stands for low Na), and the latter as HS (standing for high Na). Rectangular DC-cast ingots with dimensions of 600 × 229 × 75 mm were provided by the Arvida Research and Development Centre of Rio Tinto Aluminum, Saguenay, QC, Canada. The chemical compositions analyzed by optical emission spectroscopy are shown in Table 1.

Table 1. Chemical compositions of the DC cast AA5182 alloys (wt.%)

Alloy ID	Si	Fe	Cu	Mn	Mg	Ti	Na (ppm)
HS	0.05	0.14	≤0.05	0.25	4.8	0.023	**1.1**
LS	0.06	0.15	≤0.05	0.25	4.8	0.023	**0.3**

Rectangular blocks for the hot-rolling process, with the dimensions presented in Fig 1, were prepared from the cast ingot. The rolling faces of the blocks were machined (10 mm from each side) to remove the as-cast surface. To investigate the effect of subsurface microstructure on edge cracking, one of the short faces of each ingot was also scalped off by approximately 25 mm, while the cast surface of the other short face remained intact. The prepared blocks were subsequently homogenized using the procedure depicted in Fig. 2. One test block of each alloy was water quenched right after the homogenization treatment to study the microstructure evolution. The remaining heat-treated blocks were directly subjected to 18 consecutive passes of hot rolling. The hot rolling was carried out on a two-high rolling mill with ~310 mm roll diameter in the 400-500 °C temperature range. During hot rolling, the rolled strip temperature was constantly monitored to maintain over 400 °C. When the strip temperature fell below 400 °C, the strip was put back in the furnace to re-heat to 500 °C in-between the rolling passes. Through the rolling process, the thickness of the blocks was reduced from 75 to 3 mm with an area reduction of 96%. Samplings for further microstructural characterization were carried out after the 11th and 18th passes as well; pass #11 (plate thickness of 12 mm, 86% area reduction) was the initiation point of edge cracking detected by the naked eye, and pass #18 was the last step of the rolling process. The rolled samples of the alloy containing high sodium from the 11th and 18th passes are denoted as HS11 and HS18, respectively, while the samples of

the alloy with low sodium are referred to as LS11 and LS18, respectively. Samples which were scalped from the short surface of the ingot have a "S" appended to the end of their label (e.g., HS11S). The sample identification for the different conditions is listed in Table 2.

For the microstructure observation, an optical microscope and a scanning electron microscope (SEM, JEOL JSM-6480LV) equipped with energy dispersive spectroscopy (EDS) were used. The samples were mounted and mechanically ground using SiC papers. The polishing was subsequently carried out using alcohol-based colloidal silica suspensions to avoid any possible dissolution of Mg_2Si phase during water-based polishing. The quantitative analysis of the microstructural features was performed by the image analysis software (Clemex PE4.0). To better characterize the intermetallic particles and facilitate phase identification, the metallographic samples were etched using 0.5% HF for 10 s. However, SEM-EDS analyses were performed prior to etching.

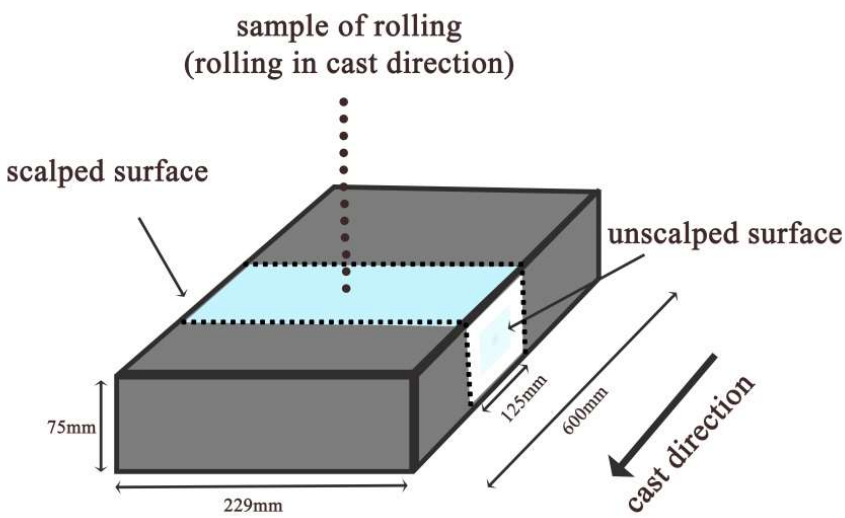

Fig. 1. Schematic of the prepared block for the hot rolling from DC-cast ingots

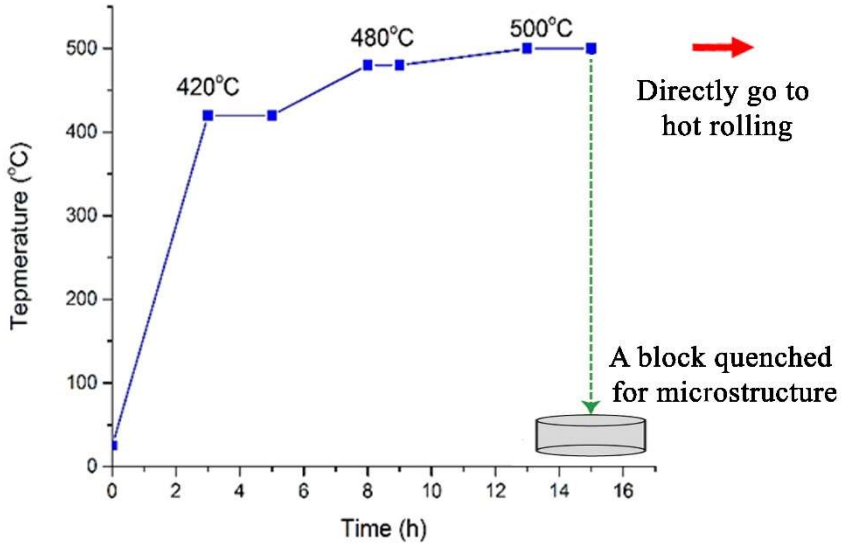

Fig. 2. Homogenization procedure applied to the DC-cast ingots

Table 1. Sample ID of rolling plates under different conditions

Alloys	#11 pass - unscalped surface	#11 pass - scalped short surface	#18 pass - unscalped surface	#18 pass - scalped short surface
HS (High Na)	HS11	HS11S	HS18	HS18S
LS (Low Na)	LS11	LS11S	LS18	LS18S

3. Results

3.1 Microstructures under as-cast and as-homogenized conditions

The edge cracks during rolling were all initiated from the subsurface region of the DC-cast ingot, and then propagated toward the ingot bulk in different extensions. Therefore, the microstructure analyses were focused on two distinct regions: the subsurface region that covers the ingot cast surface to several millimeters inwards, and the bulk region. Representative micrographs from the subsurface region are shown in Fig. 3. The cast surface from the short side of the DC-cast ingot is shown in Fig 3a. From the cast surface, the first visible zone was the inverse segregation zone, which contains enriched intermetallic particles and solute elements, as shown in Fig 3b. The inverse segregation zone had a thickness that ranged from 85 to 250 μm and could occasionally extend to approximately 400 μm. In the subsurface region, there were meniscus bands (Fig. 3a and c), which were more noticeable at the corners of the ingot and presented a repetitive pattern along the casting direction with an interval of approximately $5.5 \pm 1.5 \times 10^3$ μm. These meniscus bands brought the inverse segregation zone (enriched intermetallic particles) toward the bulk with a depth of up to approximately 800-1000 μm.

The typical as-cast microstructures of the subsurface and bulk region, displayed in Fig. 4, were composed of Mg_2Si, β-Al_8Mg_5, and Fe-rich intermetallics. Mg_2Si intermetallic particles with Chinese script morphology (Fig. 4, #1) and Fe-rich intermetallics were mostly located in the interdendrite regions. The Mg-rich β-Al_8Mg_5 particles (Fig. 4, #3) with a bulky morphology were the last eutectic intermetallic solidified in the interdendrite regions, where adequate Mg atoms were available [21,22]. The Fe-rich intermetallics appeared in three distinct types: Al_6(Mn,Fe), Al_3(Mn,Fe), and metastable Al_m(Mn,Fe); these intermetallics were characterized by SEM-EDX analysis, and were consistent with the results reported in the literature [23–26]. Al_6(Mn,Fe) particles had a plate-like morphology (Fig. 4, #4), while Al_3(Mn,Fe) particles were distinguished by a needle-like morphology (Fig. 4, #2). The metastable Al_m(Mn,Fe) particles also presented a plate-like shape and appeared only in the subsurface region (Fig.4, #5). The type and morphology of the intermetallic constituents were similar between the inverse segregation zone (Fig. 4a) and the bulk material (Fig. 4b). However, the quantity of intermetallic constituents in the inverse segregation zone was much higher than that in the bulk. The results of the quantitative image analysis indicated that the volume fraction of Mg_2Si was five times higher in the inverse segregation zone relative to the bulk, while the volume fractions of Fe-rich intermetallics and β-Al_8Mg_5 particles were two and eight times higher, respectively (Table 3). It is worth mentioning that the trace amount of Na did not affect the type and morphology of the intermetallic phases, and therefore, the results in Figs. 3 and 4 and Table 3 are valid for both high Na and low Na (HS and LS) alloys.

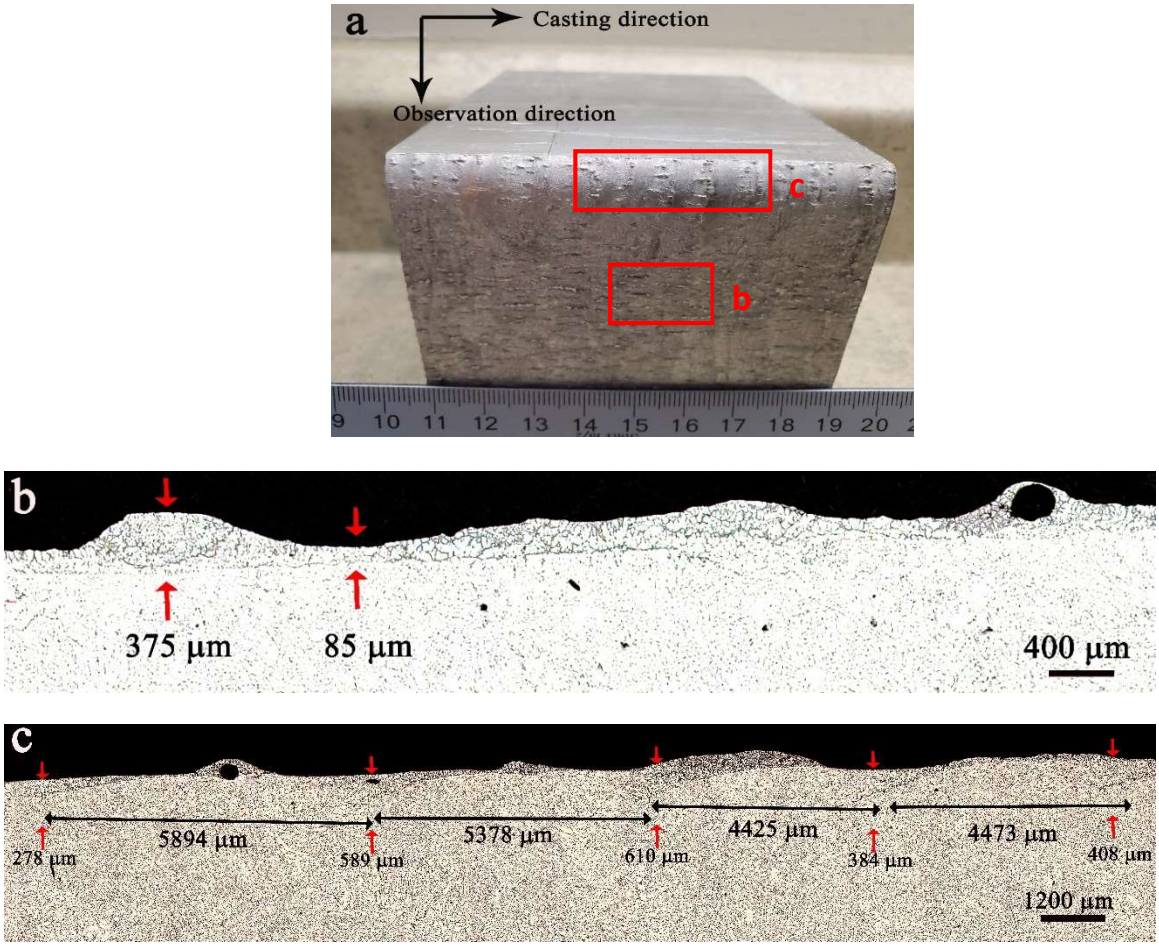

Fig. 3. The cast surface and the microstructure in the subsurface region: a) cast surface of the short side of the ingot, b) the inverse segregation zone and c) the meniscus bands.

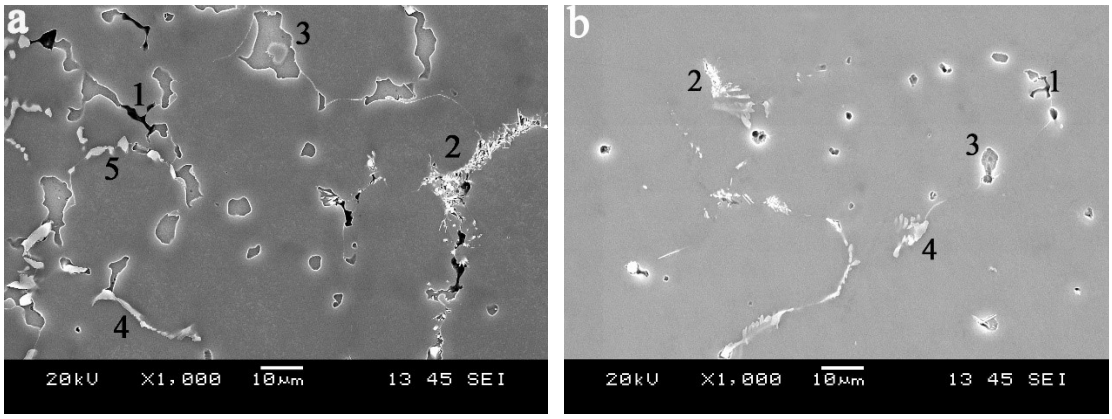

Fig. 4. SEM images of the as-cast microstructure at a) the inverse segregation zone and b) bulk: (1) Mg_2Si, (2) $Al_3(Mn,Fe)$, (3) β-Al_8Mg_5, (4) $Al_6(Mn,Fe)$, (5)$Al_m(Mn,Fe)$.

Fig. 5 shows SEM micrographs of the as-homogenized microstructure in the subsurface and bulk region. After homogenization, the β-Al_8Mg_5 intermetallics were entirely dissolved in both the subsurface and bulk region, which was in good agreement with the results reported in the literature [21]. As the β-Al_8Mg_5 eutectic phase solidified at a temperature close to 451°C, the present homogenization practice was adequate to completely dissolve these intermetallic particles. On the other hand, Mg_2Si particles were partially dissolved (close to 50%). It was reported [27] that the Mg_2Si phase changes during homogenization with the following sequences: 1) decomposition into small fragments, 2) diffusion-controlled spheroidization and 3) coarsening. Microstructural results revealed that Mg_2Si particles in this study experienced only the first two steps (the decomposition and spheroidization) without any noticeable coarsening. A limited dissolution of Mg_2Si for the alloys containing 2 wt.% Mg or higher has also been reported by Radetic et al. [28]. The Fe-rich intermetallic particles experienced only partial spheroidization, but their dissolution was negligible. It was observed that the metastable Al_m(Mn,Fe) had transformed into Al_3(Fe,Mn) during homogenization. This solid-state eutectoid phase transformation was discussed in detail by Li and Arnberg [23]. Therefore, there were two types of Fe-rich intermetallics that remained in the as-homogenized microstructure: plate-like Al_6(Mn,Fe) and needle-like Al_3(Mn,Fe) (Fig. 5). The quantitative results of the volume fraction of all intermetallics in the subsurface and bulk regions after homogenization are shown in Table 3. Although the total amount of Mg_2Si was considerably reduced during homogenization, the volume fraction of Mg_2Si was still five times higher in the inverse segregation zone than in the bulk. The amount of Fe-rich intermetallics in these samples was slightly decreased compared to the quantity in the as-cast samples, but the measured volume fraction was still two times higher in the inverse segregation zone relative to the bulk region.

Due to the large difference in the quantity of intermetallics (Mg_2Si and Fe-rich intermetallics) between the subsurface and bulk regions, the inverse segregation zone and meniscus bands were still clearly visible after homogenization. Another characteristic observed in the subsurface area of Al-Mg 5182 alloy was severe oxidization during homogenization. As shown in Fig. 6, the porous oxidized areas penetrated the cast surface inward, extending up to a few hundred micrometers into the material. The SEM-EDX results confirmed that the porous oxidized areas contained mostly AlMgO particles. Together with porosities and inclusions that were often encountered in the subsurface area (Fig. 3b), these defects provided favorable sites for the initiation of edge cracks during hot rolling.

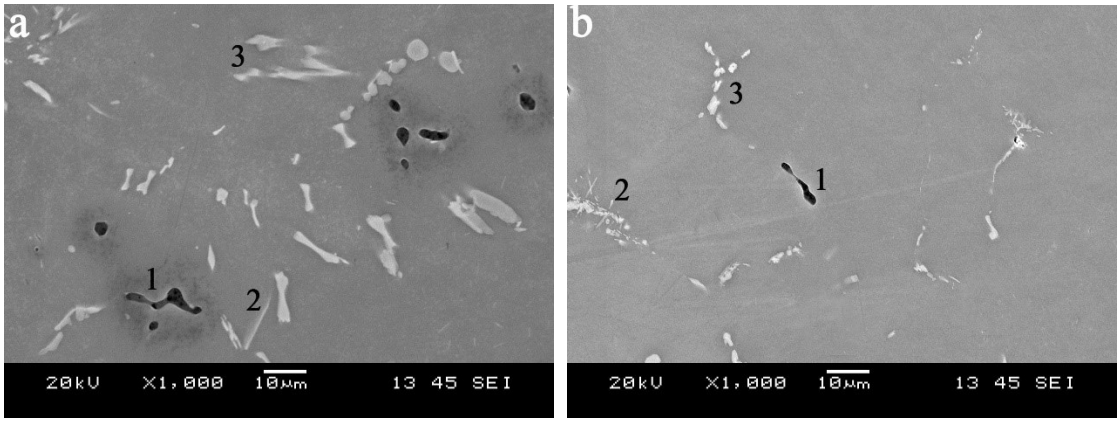

Fig. 5. SEM images of the as-homogenized microstructure at a) the inverse segregation zone and b) bulk: (1) Mg_2Si, (2) $Al_3(Mn,Fe)$ and (3) $Al_6(Mn,Fe)$.

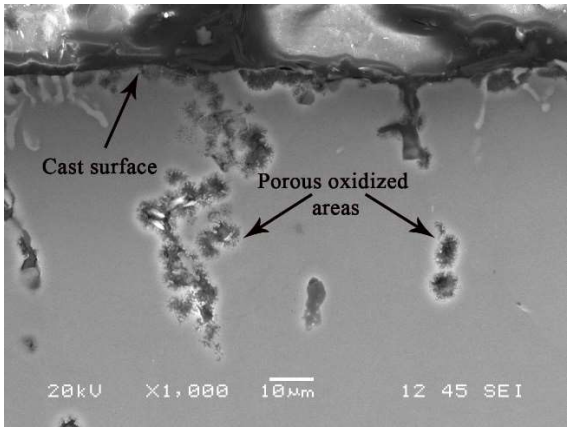

Fig. 6. Porous oxidized areas in the subsurface area of the ingot after homogenization.

Table 3. Comparison of the volume fractions of intermetallic constituents in the inverse segregation zone and bulk area (vol.%)

	As-cast			After homogenization		
	Mg_2Si	Fe-rich particles	β-Al_8Mg_5	Mg_2Si	Fe-rich particles	β-Al_8Mg_5
Inverse segregation zone	1.0	2.1	9.4	0.54	2.0	0
Bulk area	0.2	1.2	1.2	0.1	1.0	0

3.2 Edge cracking evolution during hot rolling

In the present work, the cracks in the ingot edges during hot rolling became visible by the naked eye after pass #11, with pass #18 being the final pass during hot rolling.

Therefore, the results of the rolled samples after pass #11 (with 84% area reduction) and pass #18 (with 96% area reduction) are presented here.

Cracks after pass #11 (Fig. 7a) were observed only in the sample with high Na content (HS11, Fig. 7a), and no visible cracks could be found in the sample with low Na content (LS11, Fig. 7b). By continuing the hot deformation (rolling to pass #18), the detrimental impact of Na on edge cracking susceptibility was more exposed. The macroscopic edge cracks encountered in the present work can be divided into two categories: 1) small cracks that remained superficially on the edge of the rolled strip with a maximum penetration depth of 3 mm, and 2) large cracks that were profoundly propagated into the bulk of the material. As the edges of the rolled strip are always trimmed out during the industrial rolling process, the small cracks are less harmful in terms of the rolling recovery, while the large cracks are particularly detrimental for the rolling process recovery and productivity. In the high Na sample (HS18), although the majority of the cracks were small cracks, a number of large cracks were observed on the edges and propagated up to 12-15 mm inwards (Fig. 7c and d). Furthermore, there were some triangular torn-off areas at the edges, where the cracks propagated up to 7 mm inward (Fig. 7c and d). These triangular cracks indicated the possibility of tearing off small pieces from the rolled block, which may fall out in the successive rolling passes. By moving away from the surface toward the bulk, the cracks tended to align toward the rolling direction. Another important feature of the large cracks was their repetitive pattern along the casting/rolling direction at intervals of 150 ± 20 mm, as shown in Fig. 7c. Unlike the sample HS18, in the low Na LS18 sample, no profound cracks were observed. As shown in Fig. 7e, the cracks in LS18 were all superficial with a depth of 1-3 mm, even after pass #18 with 96% reduction.

The quantity versus depth of cracks in high Na samples, measured over a 30 cm length in several samples in the rolling direction, is presented in Fig. 8. As the statistical results of Fig. 8 show, almost all cracks in the HS11 sample were small, with a maximum propagation depth of 3 mm. In the HS18 sample, a majority of the cracks (more than 80% in term of the crack number) were still small and superficial, but the rest were large and profound, with a depth of greater than 3 mm. In industrial practice, these large cracks could not only scrap the entire rolling product, but also jeopardize the rolling production line.

On the other hand, the edge cracks were mostly eliminated in the surface-scalped samples, where the side was scalped off 25 mm from the short side of the ingot. As illustrated in Fig. 9, almost no edge cracks could be found after pass #11 in both the low Na and high Na samples (Fig. 9a of LS11S and Fig. 9b of LS18S). After pass #18, no edge cracks were detectable in the low Na sample (LS18S, Fig. 9c), while a few small and superficial cracks with a depth of 1-2 mm were seen in the high Na sample (HS18S, Fig. 9d). It is important to highlight that the number of cracks in HS18S (Fig. 9d) was significantly lower even than that in the unscalped LS18 (Fig. 7e) and HS11 samples (Fig. 7a).

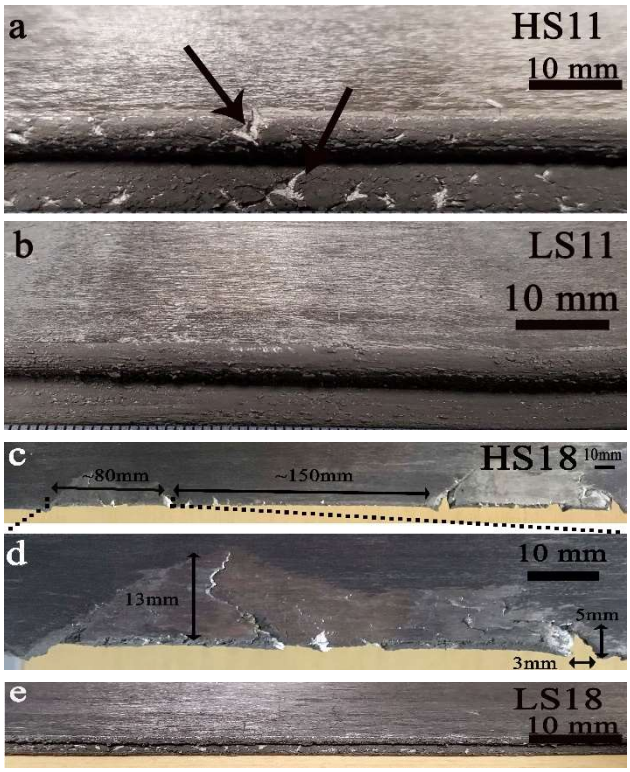

Fig. 7. The edges of high and low sodium rolled samples after passes #11 and #18 of hot rolling: a) HS11, b) LS11, c and d) HS18, e) LS18. The rolling direction is horizontal.

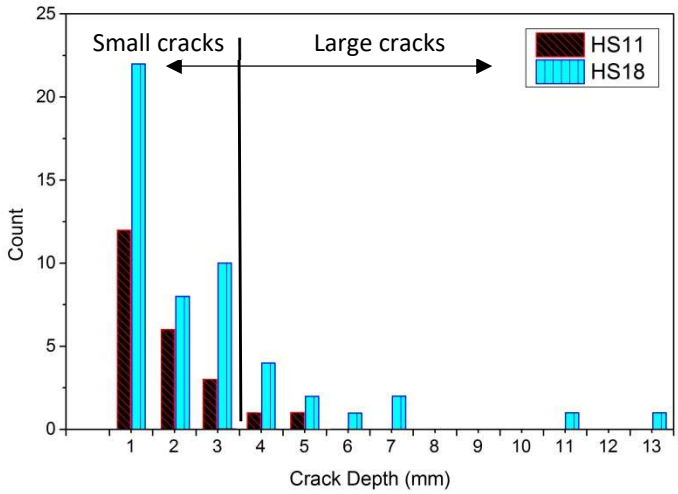

Fig. 8. Statistical data of the number and depth of edge cracks in HS11 and HS18 samples, measured over 30 cm length of rolled samples.

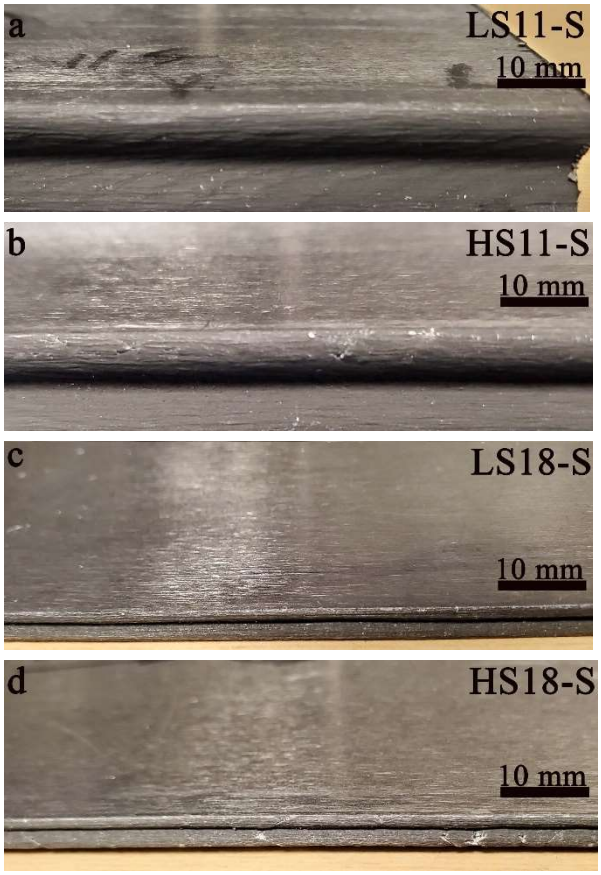

Fig. 9. The edges of the surface-scalped samples in both high and low sodium alloys after passes #11 and #18 of hot rolling: a) LS11S, b) HS11S, c) LS18 and d) HS18S.

The cracking behavior in the subsurface area was further investigated by SEM, and the results for different samples are compared in Fig. 10. The macrocracks on the edges were generally composed of numerous microcracks, and their length and width varied significantly. Although the edge cracks in the LS11 sample were not visible on the macroscale (Fig. 7b), some microcracks were still detectable, with lengths and widths of less than 50 µm and 5 µm, respectively (Fig. 10a). By applying further deformation (after pass #18), the microcracks in the LS18 sample were enlarged and had a maximum length of 100 µm and a width of up to 15 µm (Fig. 10b). These cracks were mostly limited to within 1-2 mm of the sample edge area. In the high Na HS11 sample (Fig. 10c), the cracks were remarkably larger and several times wider than those in the LS11 sample. The high Na HS18 sample showed the most severe cracking (Fig. 10d). The cracks were mostly connected to the sample surface, elongated longitudinally up to several millimeters, and branched into numerous smaller cracks along the primary crack path. The cracks/cavities were mostly inclined toward the rolling direction as they traveled from the surface toward the bulk.

Microcracks could also be found in the surface-scalped samples after passes #11 and #18 (Fig. 11). In the low Na sample (LS18S), a few microcracks were detectable in edge

area of the sample. These small microcracks did not propagate and further develop into macroedge cracks, and they were also all restricted inside the ingot subsurface region without the connection to the ingot surface (Fig. 9b). In the high Na sample (HS18S), the number of microcracks increased considerably relative to the low Na sample (LS18S). Some of them were propagated and transformed to macroscopically visible edge cracks and were also connected to the sample surface (Fig. 9d). Nevertheless, it was evident that the number, length, and width of the micro- and macrocracks in the scalped samples (Figs. 9 and 11) were very restricted and were much smaller when compared to the unscalped HS11 and HS18 samples (Figs. 7, 8, and 10).

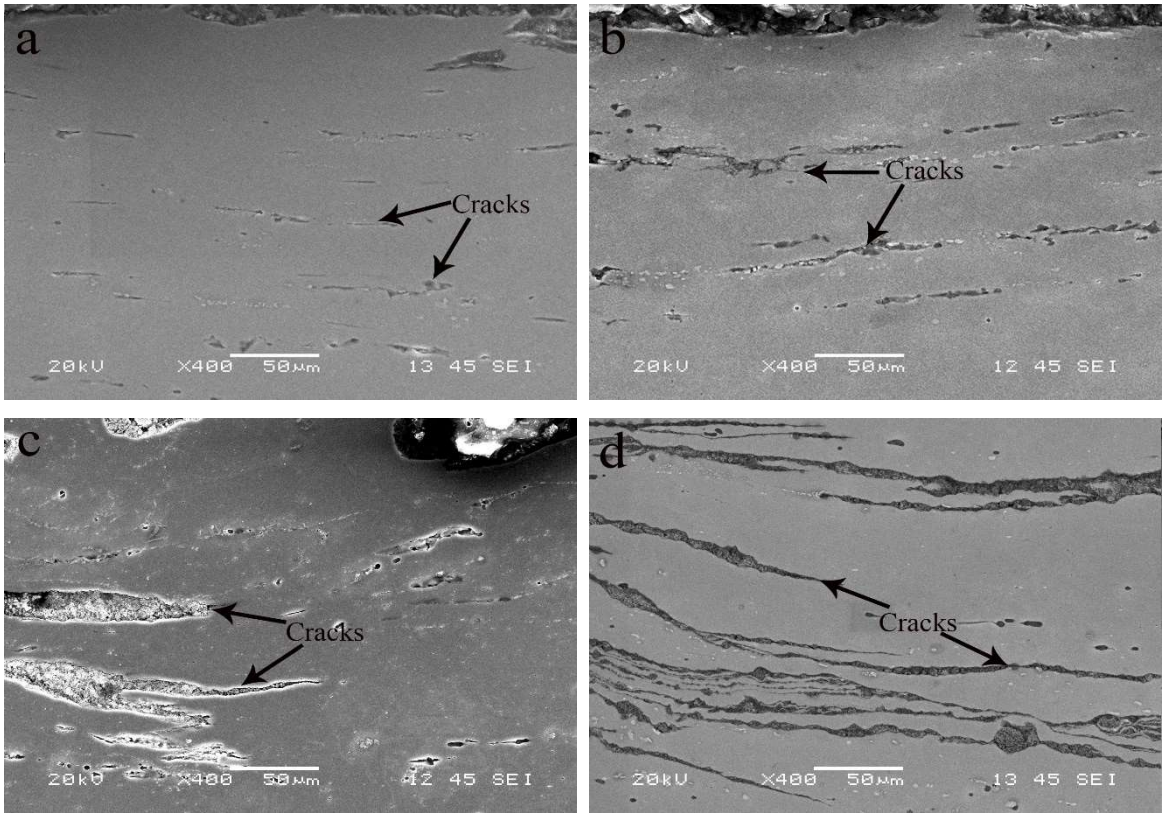

Fig. 10. SEM images of the microcracks of the rolled samples: a) LS11, b) LS18, c) HS11 and d) HS18. The top of each image is the edge of the rolled strip.

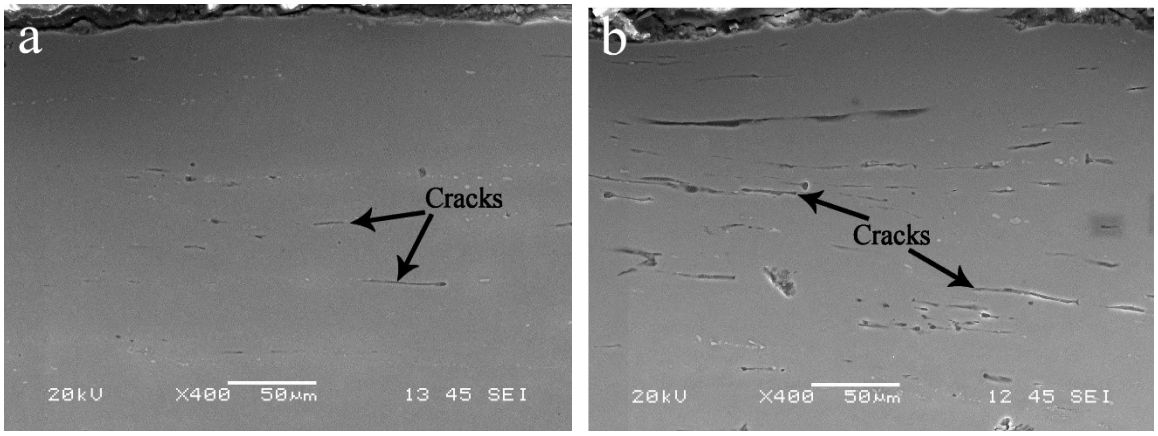

Fig. 11. SEM images of the microcracks in the surface-scalped samples: a) LS18S and b) HS18S. The top of each image is the edge of the rolled strip.

3.3 Impact of intermetallic constituents on edge cracks

As mentioned above, the β-Al_8Mg_5 intermetallics were entirely dissolved during the homogenization treatment, and Mg_2Si and Fe-rich intermetallic particles were the only intermetallic constituents remaining in the ingot microstructure during the rolling process. The Mg_2Si and Fe-rich particles in the rolled microstructure could be easily distinguished by their color, as well as by EDS analysis in SEM. In the subsurface region, Mg_2Si particles were often detached from the aluminum matrix, forming cavities/voids on their periphery adjacent to the path of the microcracks. The micrographs in Fig. 12 illustrate the debonding and cavitation of Mg_2Si particles from the Al matrix in the samples containing high Na (i.e., HS11 and HS18). In contrast to the Mg_2Si particles, Fe-rich particles underwent fragmentation during rolling, but no evidence of Fe-rich particle detachment from the aluminum matrix could be found (Fig. 12). As shown in Fig. 12, a few Fe-rich particles were also found near the Mg_2Si particle and crack path, but no decohesion of Fe-rich particles from the aluminum matrix was observed for either type of Fe-rich particles. It is evident that Fe-rich intermetallic particles did not contribute to cavitation and void formation. It is worth mentioning that at least 100 particles and the surrounding matrix were analyzed by SEM to confirm the detachment and cohesion behavior of both Mg_2Si and Fe-rich intermetallic constituents, respectively.

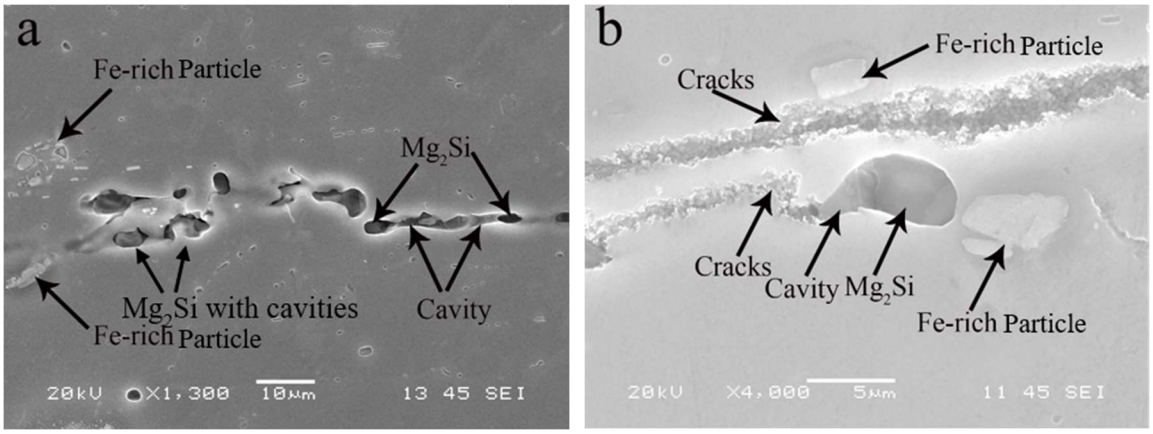

Fig. 12. SEM images of the Mg_2Si cavitation in the high Na samples: a) HS11 and b) HS18.

Results of numerous particle analyses showed that the cavities were formed in the detached area of Mg_2Si particles and extended into the matrix along the rolling direction. The phenomenon of the Mg_2Si particle-matrix decohesion and the subsequent cavitation is well depicted in Fig. 13. Figure 13a illustrates an early stage of particle debonding, with an approximately 1 μm cavity formed on one side of the Mg_2Si particle. Figure 13b presents the coalescence of several instances of Mg_2Si particle-matrix decohesion and subsequent growth to elongated cavities, leading to a path for crack propagation in the rolling direction. The particle decohesion and cavitation in the samples with high Na content (HS11 and HS18) were much more severe than in the low Na containing samples (LS11 and LS18). It is interesting to note that in both micrographs shown in Fig. 13, the Fe-rich intermetallic particles were well-bonded with the Al matrix.

During SEM observation, it appeared that not all, but a considerable number, of Mg_2Si particles detached from the Al matrix and formed cavities. To better quantify the decohesion of Mg_2Si particles and their cavitation in the samples, the distribution of the non-debonded Mg_2Si and the debonded Mg_2Si with their adjacent cavities, as well as the area fraction of Mg_2Si plus the adjacent cavities, were measured. To do so, an area of approximately 50 mm in length and a 5 mm wide was carefully scanned in 1.25 mm intervals from the surface inwards by SEM for each sample. The results are presented in each 1.25 mm interval from the surface toward the bulk material, as shown in Fig. 14. In general, the number of debonded Mg_2Si particles in the first 1.25 mm interval was the highest, and it decreased from the surface inward (Fig. 14a). Both the number density of the debonded Mg_2Si particles and the ratio of the debonded to non-debonded particles in the first 1.25 mm interval for the HS18 sample containing high Na are very high at 325 particles per mm^2 and a ratio of 2.3, respectively. In contrast, the number density of the debonded Mg_2Si particles and the ratio of the debonded and non-debonded particles for the LS18 sample containing low Na are quite low (80 particles per mm^2 with a ratio of 0.25). Furthermore, for the inside of the strip, the number densities of the debonded Mg_2Si particles of the HS18 sample are always considerably higher than those of the LS18 sample. As shown in Fig. 14b, the area fraction of debonded Mg_2Si and their associated cavities in the first 1.25 mm interval for the samples containing high Na was about three times higher

than the samples with low Na content (0.75% of HS18 vs 0.25% of LS18, and 0.5% of HS11 vs 0.18% LS11). The area fraction of the Mg_2Si cavitation became progressively smaller toward the sample inside, but the area fractions of the high Na sample (HS18 and HS11) were always higher than those of the low Na samples (LS18 and LS11).

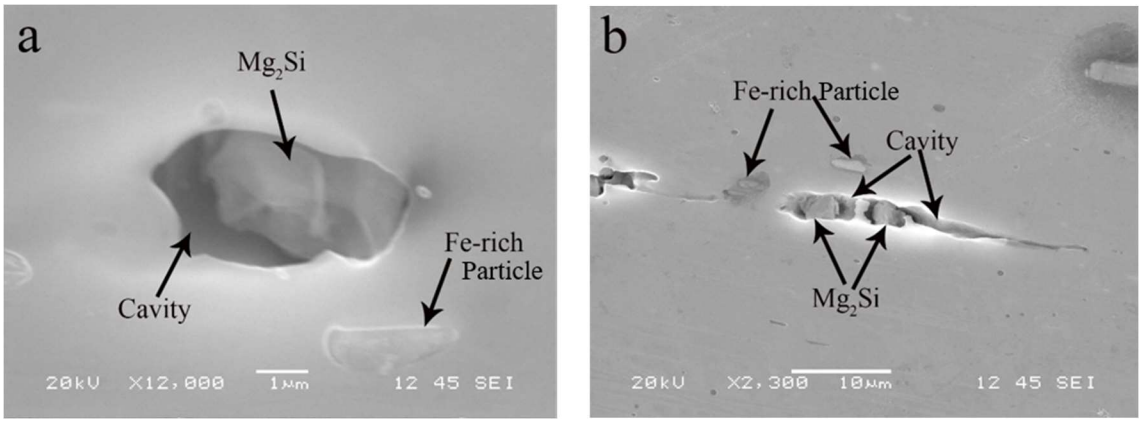

Fig. 13. Typical Mg_2Si particle-matrix decohesion and subsequent cavitation: a) an early stage of particle decohesion and b) the coalescence of cavities to form the microcrack. It is noted that the nearby Fe-rich particles were well-bonded with the matrix.

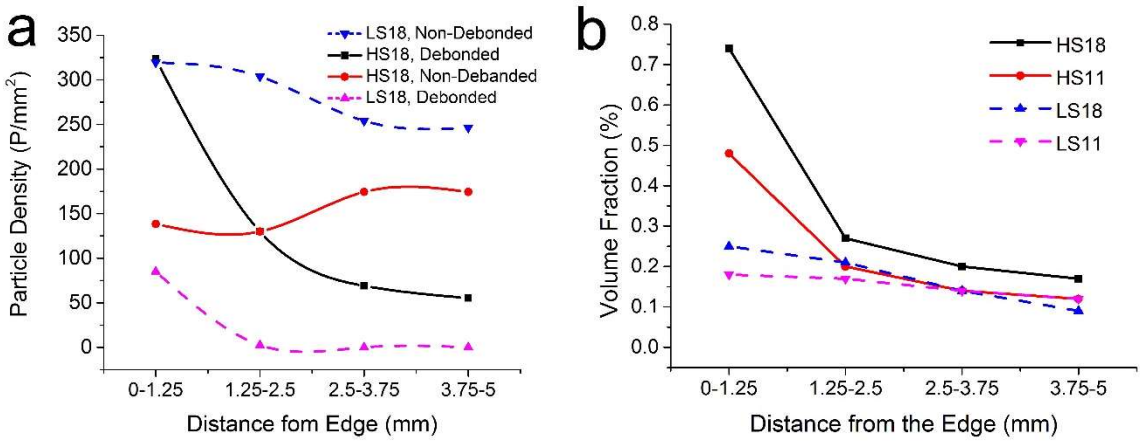

Fig. 14. Comparison of Mg_2Si particles and their cavities in the sample edge area for both rolled plates containing high and low Na, a) the distribution of the non-debonded Mg_2Si and the debonded Mg_2Si with cavity and b) the area fraction Mg_2Si particles and their cavities.

4. Discussion

During hot rolling, aluminum metal near the rolling surface of the cast ingot undergoes significantly greater deformation than the center part of the ingot. Furthermore, the essential plane-strain conditions prevail in the middle zone of the rolled ingot, while localized lateral flow occurs near the (two) edges [29]. This localized lateral flow usually results in a concave edge profile, through which the edge surface (i.e., the subsurface region of the cast ingot) is incorporated and extended into the rolling surface, as shown in Fig. 15. In successive rolling passes, the unsupported edges of the ingot strip experienced tensile stresses because of the greater elongation and bulging in the edges [5]. The applied tensile stress and the incorporation of edge surfaces into the rolling surface may create the necessary condition for crack initiation and propagation during subsequent rolling, as the material in the subsurface region had limited ductility, which may lead to macroscopic edge cracks.

The sensitivity to crack initiation and propagation at the edges of the strip is strongly dependent on the material ductility. The lower the material ductility, the more sensitive it is to the edge crack occurrence. Compared to the bulk of the material, the material ductility in the subsurface area of the cast ingot was strongly deteriorated by different defects, such as porosities and inclusions in the cast surface (Fig 3), subsurface oxidation during homogenization (Fig 6), and enriched intermetallic particles (Fig 4). Consequently, subsurface defects alongside the applied tensile stress during rolling provided favorable conditions for developing cracks. As the surface porosity, oxidation, and segregation zones were mainly driven by cast and homogenization processes rather than by alloy chemistry and impurities, subsurface crack initiation and propagation were observed in all of the LS18 and HS18 samples, regardless of Na content. Furthermore, by machining the subsurface region and removing the segregation zone and meniscus bands, the subsurface materials with limited ductility were scalped off of the ingot, and therefore, edge cracking was almost completely eliminated, occurring only near the end of the hot-rolling process (Fig. 9).

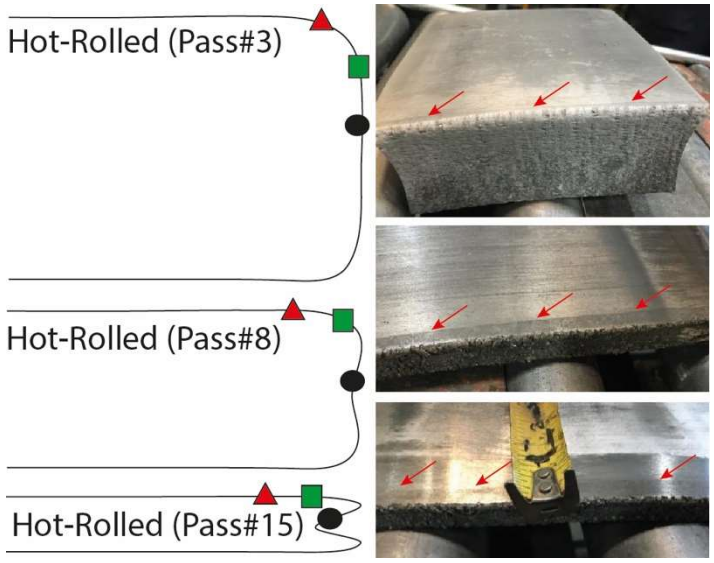

Fig. 15. Schematic of edge profile development during the reduction of hot-rolled ingot.

As mentioned above, after homogenization and prior to rolling, there were only two kinds of intermetallic constituents left in the Al matrix in both the subsurface and bulk regions: Mg_2Si and Fe-rich intermetallic particles, which were involved in plastic deformation during rolling. The subsurface region contained much more intermetallic particles than the bulk of the material (Table 3). During rolling, the Fe-rich intermetallic particles generally fragmented into small particles, but Fe-rich particles were well-bonded with the aluminum matrix, and neither decohesion from the matrix nor cavity formation were observed. It can be concluded that, although the Fe-rich intermetallic particles were twice as large in the subsurface region than in the bulk, they were not involved in the edge crack initiation and propagation. In contrast, Mg_2Si particles had a strong tendency to debond from the Al matrix and form a cavity in the Mg_2Si/Al interface under the applied tensile condition at the edges of the strip. The cavitation at the Mg_2Si particles could already be observed in pass #11, where macrocracks in HS11 and microcracks in LS11 occurred. With further deformation, the cavities grew and coalesced in both the HS18 and LS18 samples, resulting in a further loss of ductility on the edge surfaces. The development of cavitation on the periphery of the Mg_2Si particles during large-scale tensile deformation has long been observed in a similar Al-4.5Mg alloy [20], and it was found that the volume fraction of Mg_2Si cavities significantly increased with increasing strain. The microstructure analysis in the present work clearly demonstrated that the proportion of the debonded Mg_2Si with cavities and the area fraction of cavities in the high Na alloy were much higher than in the low Na alloy (Fig. 14), which is consistent with the high susceptibility of edge cracking in the high Na alloy.

The inverse segregation zone in the ingot subsurface region was generally enriched with intermetallic particles and solute elements. Simensen and Sodervall [18] investigated the trace elements in Al-4.8Mg-0.3Mn DC-cast ingots by means of microprobe analysis and secondary ion mass spectrometry. They found that the impurities (Na, Ca, etc.) were

enriched in the cast surface layer, and that a number of Na particles could be found on the surface of the intermetallic particles. Even in the homogenized and hot-rolled material, a small number of Na particles, which heterogeneously nucleated on the intermetallic particles, were detectable. Lynch [17] suggested that the high-temperature embrittlement of Al-Mg alloys could be due to the formation of low-melting-point Na-rich phases or particles. In further work by Zhang et al. [19] using thermodynamic simulation, it was found that a so-called Na-rich liquid-2 phase formed in Al-5Mg-Na system at relatively low Na concentrations, and that it exists in the 98 to 450 °C temperature range and incipiently melts at grain boundaries or other phase boundaries during hot rolling. It was concluded that the higher the Na content of the alloy, the greater the volume fraction of this low melting point phase. Regarding the Mg_2Si cavitation found in the present work, it is reasonable to assume that Na would segregate on the Mg_2Si boundaries and form a low-melting-point Na-rich thin layer or particle on the periphery of Mg_2Si particles, which underwent incipient melting during hot rolling, causing the decohesion of Mg_2Si from the matrix and subsequent cavitation. This phenomenon would be intensified in the inverse segregation zone of the alloy with high Na level, as the inverse segregation zone contained much more Mg_2Si particles (several times more than the bulk of the material in the present study alloy) and a high amount of segregated Na was also available. It is evident that numerous debonded Mg_2Si particles contaminated with Na in the ingot subsurface region provided favorable conditions for crack initiation and propagation, provoking the occurrence of macro-scale edge cracking.

This hypothesis can explain the occurrence of numerous superficial, small edge cracks – a majority of the cracks – that remained on the edges of the strip. It is still difficult to explain the development of large edge cracks that can extend several dozen millimeters from the edge into the bulk when taking into account the limited thickness of the inverse segregation zone (100-300 μm) and the significant reduction in the number of Mg_2Si particles with increasing distance from the edge (Fig. 14). However, the meniscus bands brought the inverse segregation zone with enriched Mg_2Si particles deeper toward the bulk (several times deeper than the segregation zone self), as shown in Fig. 3c. Utilizing the same cause and process as Mg_2Si cavitation, the debonded Mg_2Si particles contaminated with Na that existed along the penetrating meniscus bands provided favorable paths for large crack propagation. Fig. 16 shows an example where the Mg_2Si particles and the associated coalesced cavities can be found along the crack path and in the crack tip in a large and widely opened edge crack. The large and profound cracks, which were mainly seen in HS18 samples, presented a repetitive pattern with an interval of 150 ± 20 mm along the rolling direction. A number of microstructure analyses were performed to determine the possible correlation of the edge cracks with the subsurface microstructure. The contribution of the meniscus bands to the large and profound cracks can be determined from the following two facts, in addition to the much deeper Mg_2Si cavitation into the bulk material induced by the meniscus bands. First, considering the approximately 25 times elongation applied in the rolling direction after pass #18, the interval of the large and profound cracks (150 ± 20 mm) is in satisfactory agreement with the intervals of meniscus bands (5.5 ± 1.5 mm). Second, after scalping the cast surface layer on the short side of the

ingot to remove all the inverse segregation zone and meniscus bands, the large and profound cracks completely disappeared, and the small and surficial cracks were reduced significantly (Fig. 9).

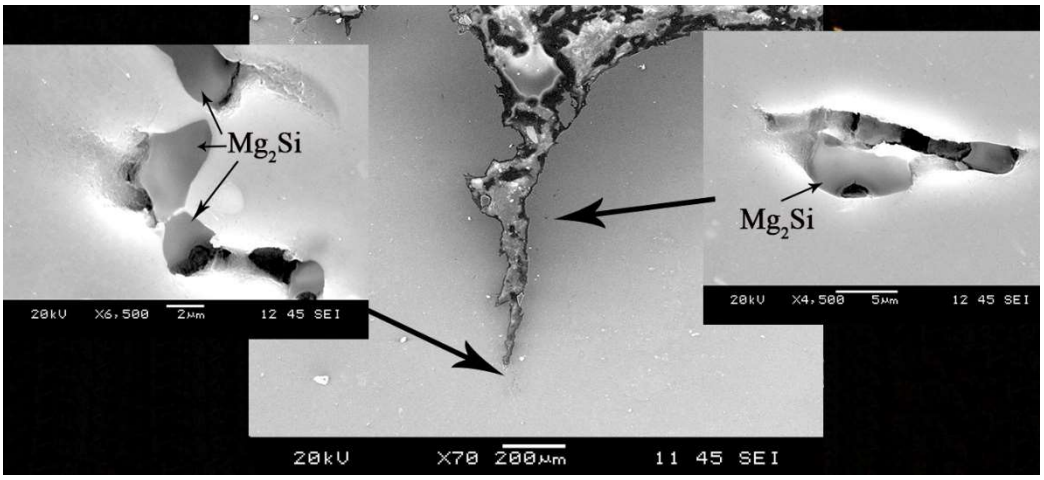

Fig. 16. Observation of Mg_2Si cavitation on an HS18 sample where the Mg_2Si particles and their associated, coalesced cavities were detected both along the crack path and in the crack tip.

Several researchers reported that the Na-induced cracks were intergranular, owing to the segregation of Na on the aluminum grain boundaries [12,15,16]. In our observation, many edge cracks were found to be a mixture of intergranular and transgranular in nature. The large crack shown in Fig. 17 was intergranular in the middle and transgranular near the end of the path. The small crack at the right bottom of Fig. 17 was transgranular, and the thin crack on the left side was mainly intergranular. As mentioned above, Mg_2Si particles precipitated in the interdendrite regions during solidification, which might be in the interiors of the aluminum grain or in the aluminum grain boundaries. Therefore, the Mg_2Si cavitation, as discussed above, may provide a reasonable explanation for the intergranular and transgranular propagation of the edge cracking. On the other hand, considering that a portion of the Mg_2Si particles that originated from solidification were dissolved during homogenization, the low-melting-point Na-rich layer on the periphery of Mg_2Si particles could have dissolved back to the matrix and segregated along the aluminum grain boundaries, leading to the intergranular propagation of the crack.

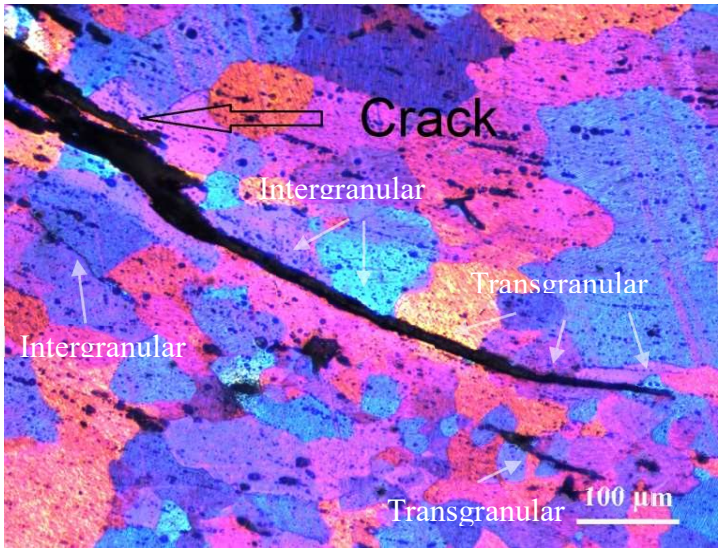

Fig. 17. The edge cracks display the mixing of intergranular and transgranular propagation in HS18 sample. The grain structure was revealed under polarized optical microscopy using electrochemically etching in Barker solution.

5. Conclusions

The occurrence of edge cracks during pilot-scale casting and hot rolling trials of AA5182 aluminum alloys containing two levels of Na were investigated. The present work focused on the impact of the intermetallic constituents in the DC-cast ingot on sodium-induced edge cracking. The following conclusions can be drawn:

1. After homogenization of the DC-cast ingots, two main intermetallic constituents remained in the ingot microstructure: Fe-rich intermetallic particles and Mg_2Si particles. The amount of Fe-rich intermetallics was two times higher and the volume of Mg_2Si particles was five times higher in the inverse segregation zone of the ingot subsurface region than in the bulk of the material.

2. During hot rolling, neither decohesion of the Fe-rich intermetallic particles from the aluminum matrix nor cavity formation were observed, indicating the absence of Fe-rich intermetallic particles in the crack initiation and propagation process. In contrast, Mg_2Si particles had a strong tendency to debond with the matrix and form cavities in the Mg_2Si/Al interface at the edges of the rolled strip. The Mg_2Si cavitation in the high Na alloy was much more severe than that in the low Na alloy.

3. Sodium promoted the Mg_2Si cavitation, most likely due to the segregation of Na on the periphery of the Mg_2Si particles, resulting in the high susceptibility of edge cracking in the high Na alloy. Numerous debonded Mg_2Si particles contaminated with Na in the

ingot subsurface region provided favorable conditions for crack initiation and propagation.

4. The large edge cracks with a repetitive pattern could be related to the meniscus bands on the cast ingot surface. The meniscus bands moved the inverse segregation zone, along with the enriched Mg_2Si particles, deeply toward the bulk. The debonded Mg_2Si particles and their cavitation along the penetrated meniscus bands provided favorable paths for large crack propagation, which were particularly detrimental to the rolling recovery and process.

5. Removing the segregated zones and meniscus bands on the short side of DC-cast ingots or reducing the Na content can significantly reduce the edge cracking susceptibility.

Acknowledgements

The authors would like to acknowledge the financial support of the Natural Sciences and Engineering Research Council of Canada (NSERC) and Rio Tinto Aluminum through the Research Chair in the Metallurgy of Aluminum Transformation at University of Quebec in Chicoutimi.

Disclosure statement

No potential conflict of interest was reported by the author(s).

Funding

This work was supported by the Natural Sciences and Engineering Research Council of Canada under Grant No. CRDPJ 514651-17.

References

[1] J. Hirsch, *Recent development in aluminium for automotive applications*, Trans. Nonferrous Met. Soc. China (English Ed. 24 (2014), pp. 1995–2002.

[2] W.S. Miller, L. Zhuang, J. Bottema, A.J. Wittebrood, P. De Smet, A. Haszler, et al., *Recent development in aluminium alloys for the automotive industry*, Mater. Sci. Eng. A 280 (2000), pp. 37–49.

[3] J. Hirsch, *Aluminium in Innovative Light-Weight Car Design*, Mater. Trans. 52 (2011), pp. 818–824.

[4] P. Thomson and N. Burman, *Edge cracking in hot-rolled Al-Mg alloys*, Mater. Sci. Eng. 45 (1980), pp. 95–107.

[5] N.M. Burman and P.F. Thomson, *Edge cracking and profile of hot rolled aluminum slabs*, J. Mech. Work. Technol. 13 (1986), pp. 205–217.

[6] H. Riedel, F. Andrieux, T. Walde and K. Karhausen, *The Formation of Edge Cracks during Rolling of Metal Sheet*, Steel Res. Int. 78 (2007), pp. 818–824.
[7] D.G. Eskin and L. Katgerman, *Macrosegregation Mechanisms in Direct-Chill Casting of Aluminium Alloys*, Mater. Sci. Forum 630 (2010), pp. 193–199.
[8] R. Nadella, D.G. Eskin, Q. Du and L. Katgerman, *Macrosegregation in direct-chill casting of aluminium alloys*, Prog. Mater. Sci. 53 (2008), pp. 421–480.
[9] J.F. Grandfield and P.T. McGlade, *DC casting of aluminium: Process behaviour and technology*, Mater. Forum 20 (1996), pp. 29–51.
[10] N. Bayat and T. Carlberg, *Surface structure formation in direct chill (DC) casting of al alloys*, Jom 66 (2014), pp. 700–710.
[11] C.E. Ransley and D.E.J. Talbot, *The embrittlement of aluminium magnesium alloys by sodium*, J. Inst. Met. 88 (1959), pp. 150–158.
[12] G.H. Lu, Y. Zhang, S. Deng, T. Wang, M. Kohyama, R. Yamamoto et al., *Origin of intergranular embrittlement of Al alloys induced by Na and Ca segregation: Grain boundary weakening*, Phys. Rev. B - Condens. Matter Mater. Phys. 73 (2006), pp. 1–5.
[13] H. Yamada, K. Horikawa and H. Kobayashi, *Effect of trace sodium on high temperature embrittlement in quasi-static and impact deformation of Al–5 mass% Mg alloys*, J. Japan Inst. Light Met. 60 (2010), pp. 31–35.
[14] S. Zhang, O.Y. Kontsevoi, A.J. Freeman and G.B. Olson, *Sodium-induced embrittlement of an aluminum grain boundary*, Phys. Rev. B - Condens. Matter Mater. Phys. 82 (2010), .
[15] S. Zhang, O.Y. Kontsevoi, A.J. Freeman and G.B. Olson, *Aluminum grain boundary decohesion by dense sodium segregation*, Phys. Rev. B - Condens. Matter Mater. Phys. 85 (2012), pp. 1–8.
[16] K. Horikawa, S. Kuramoto and M. Kanno, *Intergranular fracture caused by trace impurities in an Al–5.5 mol % Mg alloy*, Acta Mater. 49 (2001), pp. 3981–3989.
[17] S.P. Lynch, *Comments on Intergranular fracture caused by trace impurities in an Al-5.5 mol% Mg alloy*, Acta Mater. 47 (2002), pp. 125–129.
[18] C.J. Simensen and U. Södervall, *Investigation of trace elements in an Al-4.8 wt.% Mg-0.3 wt.% Mn alloy*, Surf. Interface Anal. 30 (2000), pp. 309–314.
[19] S. Zhang, Q. Han and Z.K. Liu, *Fundamental understanding of Na-induced high temperature embrittlement in Al-Mg alloys*, Philos. Mag. 87 (2007), pp. 147–157.
[20] H. Hosokawa, H. Iwasaki, T. Mori, M. Mabuchi, T. Tagata and K. Higashi, *Effects of Si on deformation behavior and cavitation of coarse-grained Al-4.5Mg alloys exhibiting large elongation*, Acta Mater. 47 (1999), pp. 1859–1867.
[21] O. Engler and S. Miller-Jupp, *Control of second-phase particles in the Al-Mg-Mn alloy AA 5083*, J. Alloys Compd. 689 (2016), pp. 998–1010.
[22] O. Engler and J. Hirsch, *Control of recrystallisation texture and texture-related properties in industrial production of aluminium sheet*, Int. J. Mat. Res. 100 (2009), pp. 564–575.
[23] Y.J. Li and L. Arnberg, *A eutectoid phase transformation for the primary intermetallic particle from Alm(Fe,Mn) to Al3(Fe,Mn) in AA5182 alloy*, Acta

Mater. 52 (2004), pp. 2945–2952.
[24] Y.J. Li and L. Arnberg, *Solidification structures and phase selection of iron-bearing eutectic particles in a DC-cast AA5182 alloy*, Acta Mater. 52 (2004), pp. 2673–2681.
[25] G. Yi, B. Sun, J.D. Poplawsky, Y. Zhu and M.L. Free, *Investigation of pre-existing particles in Al 5083 alloys*, J. Alloys Compd. 740 (2018), pp. 461–469.
[26] A. Poznak, D. Freiberg and P. Sanders, *Automotive Wrought Aluminium Alloys*, Elsevier Ltd., 2018.
[27] M.A. Moustafa, F.H. Samuel and H.W. Doty, *Effect of solution heat treatment and additives on the microstructure of Al-Si (A413.1) automotive alloys*, J. Mater. Sci. 38 (2003), pp. 4507–4522.
[28] T. Radetić, M. Popović and E. Romhanji, *Microstructure evolution of a modified AA5083 aluminum alloy during a multistage homogenization treatment*, Mater. Charact. 65 (2012), pp. 16–27.
[29] L.S. Bayoumi, *Edge stresses in wide strip hot rolling*, Int. J. Mech. Sci. 39 (1997), pp. 397–408.